

Article

Chemical Bonding of AlH₃ Hydride by Al-L_{2,3} Electron Energy-Loss Spectra and First-Principles Calculations

Kazuyoshi Tatsumi ^{1,*}, Shunsuke Muto ¹, Kazutaka Ikeda ² and Shin-Ichi Orimo ³

¹ Department of Materials, Physics and Energy Engineering, Nagoya University, Chikusa, Nagoya 464-8603, Japan; E-Mail: s-mutoh@nucl.nagoya-u.ac.jp

² Institute of Materials Structure Science, High Energy Accelerator Research Organization (KEK), 1-1 Oho, Tsukuba, Ibaraki 305-0801, Japan; E-Mail: kikeda@post.j-parc.jp

³ Institute for Materials Research, Tohoku University, Sendai 980-8577, Japan; E-Mail: orimo@imr.tohoku.ac.jp

* Author to whom correspondence should be addressed; E-Mail: k-tatsumi@nucl.nagoya-u.ac.jp; Tel.: +81-52-789-5135; Fax: +81-52-789-5137.

Received: 30 January 2012; in revised form: 20 March 2012 / Accepted: 22 March 2012 /

Published: 30 March 2012

Abstract: In a previous study, we used transmission electron microscopy and electron energy-loss (EEL) spectroscopy to investigate dehydrogenation of AlH₃ particles. In the present study, we systematically examine differences in the chemical bonding states of Al-containing compounds (including AlH₃) by comparing their Al-L_{2,3} EEL spectra. The spectral chemical shift and the fine peak structure of the spectra were consistent with the degree of covalent bonding of Al. This finding will be useful for future nanoscale analysis of AlH₃ dehydrogenation toward the cell.

Keywords: AlH₃; chemical bonding; EELS; first principles calculation

1. Introduction

Aluminum trihydride (AlH₃, alane) has high gravimetric and volumetric hydrogen densities (10 wt % and 149 kg-H₂/m³, respectively). It has been investigated for hydrogen storage applications [1–3] after Sandrock *et al.* reported that ball-milling with small amounts of LiH sufficiently accelerated its dehydrogenation kinetics to enable it to be used as an onboard power supply for vehicles [1]. To reveal

the mechanism for this accelerated dehydrogenation, it is desirable to analyze the chemical bonding changes of the system on at least sub-micron order.

After the report of Sandrock *et al.*, aluminum trihydride has been intensively studied both experimentally and theoretically. In particular, its high pressure phases and phase stabilities have been investigated theoretically [4–6] and experimentally [3,6,7]. A theoretical search was conducted for AlH_3 crystal structures and two crystal structures were proposed: the β and γ - AlH_3 phases [4]. The crystal structures of the β [8] and γ [9] phases were subsequently analyzed experimentally. The calculated electronic structures (including chemical bonding) of the polymorphs and/or other hydrides have been compared [4,10]. However, apart from reference [11], there have been no experimental studies of their electronic structures. Chemical bonding around H atoms in solid materials cannot be directly investigated by X-ray or electron spectroscopy due to the low scattering powers of H for both x-rays and electrons. In contrast, chemical bonding in compounds in the Al–H–Na system have been theoretically investigated [4]. Alternatively, as has been done only in reference [11], spectroscopic information about the counter element Al in several Al-containing compounds can be systematically investigated to determine the basic chemical bonding of AlH_3 with the aid of theoretical electronic structure calculations.

We recently investigated dehydrogenation of AlH_3 by transmission electron microscopy (TEM) and electron energy loss spectroscopy (EELS) [12,13]. We obtained TEM images and electron diffraction patterns during dehydrogenation. Moreover, EELS (including Al core-electron excitation spectra) revealed that single hydride crystals were coated with a thin amorphous alumina layer.

The present study extends this earlier study by investigating the relationship between Al EEL spectra and the chemical bonding of Al in the hydride and other Al-containing compounds. Because the electron energy loss near-edge structure (ELNES) reflects the local electronic structure around the excited atom in the illuminated area, the relationship obtained will provide basic information for future EELS analysis of the change in the local chemical bonding that is responsible for accelerating dehydrogenation.

2. Results and Discussion

2.1. Al- $L_{2,3}$ EELS

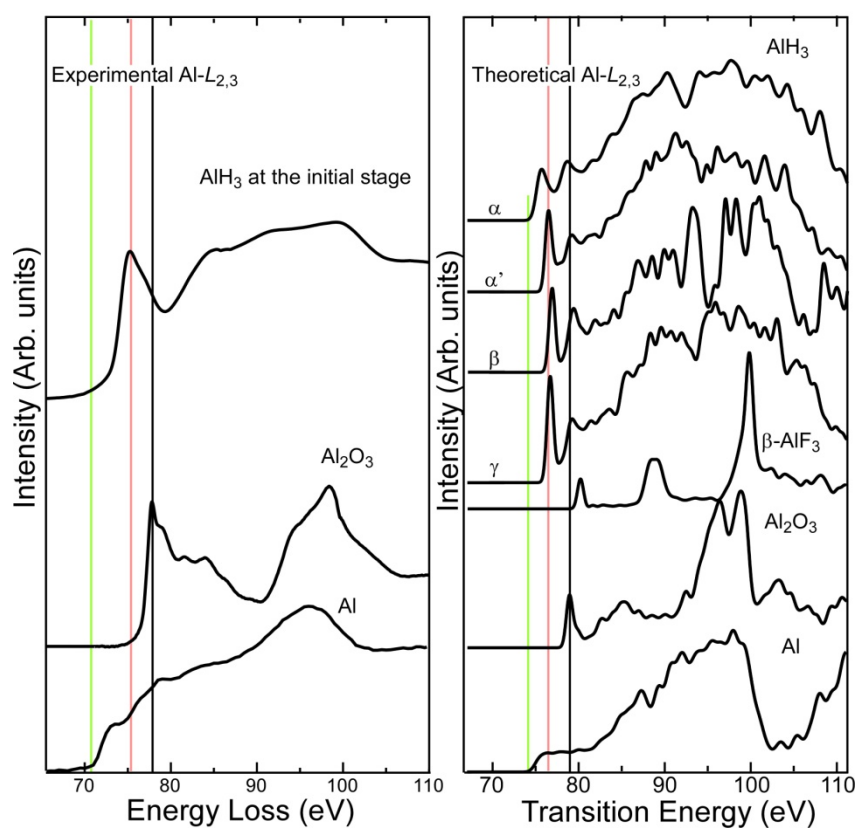
Figure 1 shows experimental and theoretical Al- $L_{2,3}$ spectra of AlH_3 . For reference, it also shows experimental spectra of Al_2O_3 and Al to evaluate how well the theoretical calculations reproduce the spectra. Theoretical spectra were calculated for four different AlH_3 phases (α , α' , β , and γ), typical aluminum compounds (Al_2O_3 and Al), and β - AlF_3 , which has the same crystal structure as α' - AlH_3 .

The peak profiles, positions, and chemical shifts of the threshold in the experimental and theoretical ELNES of metallic Al and Al_2O_3 are in reasonable agreement, although the intensities on the lower energy side (*i.e.*, from the onset of ionization to 10 eV) of the theoretical spectra tend to be smaller than those of the experimental spectra. This underestimation may be a result of excitonic effects beyond the one-electron approximation due to the relatively shallow core-shell excitation [14–16]. The characteristics of the experimental spectrum of the hydride are qualitatively consistent with those of the theoretical spectrum. We were unable to identify the phase of the hydride sample from the spectral data because the pre-peak intensities are not very reliable in the theoretical spectra. A higher

experimental energy resolution and improved theoretical reproducibility are desirable for phase identification.

To clarify the most characteristic features of the spectral data and the chemical shifts of the Al compounds, the vertical green, red and black lines in Figure 1 respectively indicate the energy positions of the onset for the metallic Al spectrum, and the first peaks in the hydride and Al₂O₃ spectra. The calculations correctly reproduce their experimental order. The energy of the first peak in the theoretical β -AlF₃ spectrum (80.2 eV) is higher than that of Al₂O₃ (79.0 eV) by half the energy difference between AlH₃ and Al₂O₃ (2.5 eV).

Figure 1. Experimental (a) and theoretical (b) Al-*L*_{2,3} energy loss near-edge structure (ELNES) of AlH₃ and reference compounds. The vertical green, red, and black lines indicate the energy positions of the onset of metallic Al spectrum, the first peak of AlH₃ and the first peak of Al₂O₃, respectively.

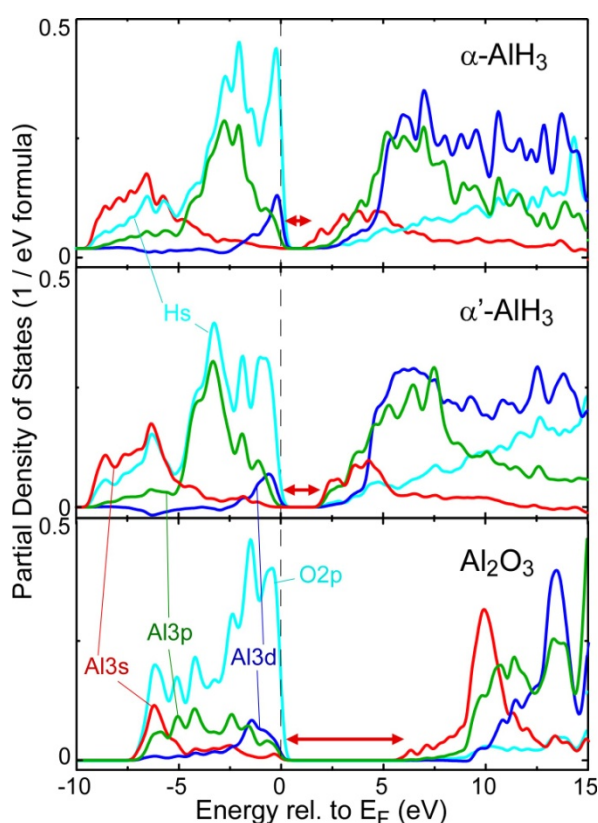


2.2. Electronic Structure near the Band Gap

The hydride and other compounds are expected to have different theoretical ground-state electronic structures near the band gap and different chemical bonding: these differences are thought to give rise to the observed chemical shifts in the EELS Al-*L*_{2,3} spectra. Figure 2 shows the partial density of states (PDOS) near the band-gap for α , α' -AlH₃, and Al₂O₃. The band gap widths indicated by the double-headed arrows are respectively 1.4, 2.1, and 5.9 eV for α , α' -AlH₃, and Al₂O₃, indicating that the chemical bonding of AlH₃ is less ionic than that of Al₂O₃. In contrast, the experimentally observed band gap is about 9 eV for Al₂O₃. Thus, the present calculation significantly underestimates the band-gap energy, which is common for calculations based on the local density approximation.

Improved techniques for calculating the electronic exchange and correlation potential such as the self-interaction-corrected local density approximation [17] are more promising for accurately reproducing the chemical shifts between metallic and insulating compounds; we intend to use such a method in a future study. In AlH_3 PDOS, the valence bands mainly consist of hydrogen orbitals, indicating that H is anionic. Nevertheless, the contribution of the Al orbitals to the valence bands is greater in AlH_3 than in Al_2O_3 . In contrast, the conduction bands are mainly formed by Al orbitals, which are more hybridized with anion (H) orbitals in the hydride than the anion (O) orbitals in the oxide. These compositional differences in the valence and conduction bands confirm that AlH_3 is less ionic than Al_2O_3 .

Figure 2. Calculated partial density of states (PDOS) for α - AlH_3 and Al_2O_3 . The energy is relative to the Fermi level. The double-headed arrows indicate the band gaps of the electronic structures.



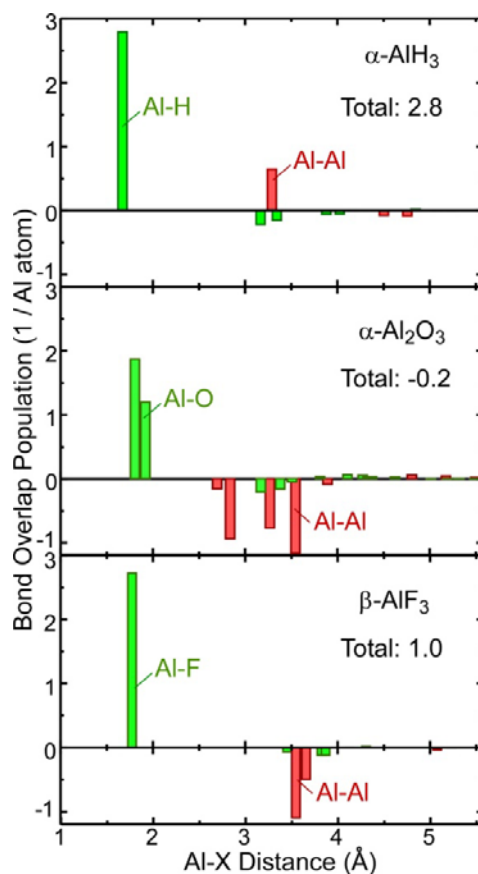
The measured $\text{Al-L}_{2,3}$ spectra reflect the unoccupied PDOS of Al s and d symmetry orbitals under the electric dipole approximation. For both AlH_3 and Al_2O_3 , the Al $3s$ orbital is dominant over the Al $3d$ orbital at the bottom of the conduction bands. Therefore, the first peaks in the spectra in Figure 1 are roughly assigned to the lower energy states of Al $3s$ bands. The relative energy of the bottom of the conduction bands of α and α' - AlH_3 with respect to the Al $2p$ inner level is 2.7 (2.1) eV lower than that of the oxide. Since this energy difference is comparable to the experimental chemical shift between these compounds, the difference in the Al ionicity of the theoretical ground electronic structure can well explain the experimental chemical shift. Chemical bonding is discussed in detail in the next section.

The differences between the two hydride polymorphs are rather small. The other hydride phases, which are not shown in Figure 2, had similar PDOS to that of the α' phase. At the conduction band bottom, Al $3p$ is less hybridized with Al $3s$ in the α phase than in the α' and the other hydride phases. This might be responsible for the differences in the pre-peak structures of the polymorphs in the theoretical Al $L_{2,3}$ ELNES, although the incorporated excitonic effects should be more rigorously considered.

2.3. Covalent Bond Strength

To investigate the covalent bond strength between the Al and its neighboring atoms, Figure 3 plots the bond overlap population (BOP) between each atom pair with respect to the interatomic distance. A positive BOP indicates that the covalent bond charge accumulates between the atom pair. On the other hand, a negative BOP indicates that the electron charge between the atoms is deficient relative to that of the superposed atomic electron densities, which is regarded as an antibonding mechanism between the atoms. The hydride contains a significant covalent bond charge for both Al–Al and Al–H. In contrast, Al_2O_3 has large negative BOPs for Al–Al, resulting in a negative total BOP of -0.2 per Al atom. This result implies that an alternative mechanism, namely an ionic bonding mechanism, is dominant for Al_2O_3 . $\beta\text{-AlF}_3$ has a similar interatomic distance distribution to that of $\alpha\text{-AlH}_3$, which is consistent with $\beta\text{-AlF}_3$ having an identical crystal structure to $\alpha'\text{-AlH}_3$. However, unlike for the hydride, all Al–Al pairs have negative BOPs.

Figure 3. Plots showing the calculated bond overlap population (BOP) and the corresponding atomic distances between an Al atom and its near neighbors. The number in each graph indicates the sum of the BOPs.



2.4. Comparison of Chemical Bonding between the Al-Containing Compounds

Table 1 lists the theoretical band-gap energy, the Al effective charge, and the sum of BOPs for Al–X (X = Al, H, O, F) to characterize the chemical bonding of the calculated Al compounds. The other hydride phases, which are not shown in Table 1, had similar values to those of the α and α' phases. The Al effective charge represents the number of valence electrons belonging to the Al orbitals. A value smaller than 3 indicates cationic Al. In all of the three rows, the values for the hydrides are intermediate between those of metallic Al and Al₂O₃. The ionic bonding or the covalent bond strengths of the hydrides are intermediate between those of Al and Al₂O₃.

Except for the smallest BOP of Al₂O₃, the listed data indicate stronger ionic bonding toward the right-hand side. The exception may be ascribed to the crystal structure, since the Al–Al distances are much shorter in Al₂O₃ than in the hydride and fluoride (see Figure 3). The significant overlap between the Al orbitals and their antibonding interactions results in the lowest total BOP.

The threshold of the Al–L_{2,3} edges in Figure 1 is shifted in a manner that is consistent with the overall trend for the chemical bonding in the compounds. In the theoretical spectrum of metallic Al, we can see a number of small peaks located continuously. In contrast, the number of fine peaks in the spectra decreases in the order AlH₃, Al₂O₃, and AlF₃ with increasing peak intensities and peak distances. Thus, the consistency between the spectra and theoretical data in Table 1 indicates that both the chemical shift and the fine peak structure of the Al–L_{2,3} spectra may be experimental indicators for the degree of covalent bonding in the Al-containing compounds. These indicators may help clarify the chemical bonding changes of AlH₃ in a localized area (for example, changes during the accelerated dehydrogenation).

Table 1. Comparison of calculated band gap, effective charge, and BOP of Al-containing compounds (including AlH₃).

	Al	AlH ₃ (α , α')	Al ₂ O ₃	AlF ₃
LDA band gap (eV)	0.0	1.4, 2.1	5.9	7.2
Al effective charge	3.0	2.8, 2.8	2.1	1.8
Sum of BOP Al–X (1/Al atom)	3.6	2.9, 2.7	−0.2	1.0

3. Experimental and Theoretical Section

3.1. EELS Measurements

The observed hydride sample was prepared by the chemical reaction between LiAlH₄ and AlCl₃ in an ether (99.5% purity Et₂O) solution. Prior to preparing TEM specimens, we confirmed that the powder x-ray diffraction pattern of the sample was that of α -AlH₃ [3,12]. Further details about the sample preparation and characterization are given in references [12,13].

Electron-irradiation-induced dehydriding of AlH₃ has been observed [13]. A single crystal of AlH₃ was decomposed into metallic Al nanoparticles, while its external shape remained almost unchanged. We carefully measured EELS from the hydride by reducing the electron dose to be sufficiently low to avoid its instantaneous decomposition and also to identify the phase by electron diffraction and EELS. Al–L_{2,3} ELNES was then isolated after subtracting the pre-edge background by a power law. Since the

Al- $L_{2,3}$ ELNES of the hydride has a very low signal to noise ratio (<5) due to the low electron dose, the spectrum were processed by the Pixon method [18] to remove statistical noise.

3.2. Theoretical Calculations

The theoretical ELNES was calculated by first-principles calculations with a local approximation to the density functional theory so as to investigate the chemical bonding between Al and its surrounding atoms. Prior to the spectral calculations, the crystal parameters of the structures were fully optimized by another first-principles procedure, the projected augmented-wave method [19,20] to reduce the computational cost. For the theoretical ELNES calculation, we adopted the orthogonalized linear combination of atomic orbital (OLCAO) band method [21] because the atomic orbital basis of the method straightforwardly provides the chemical bonding of the structures, as described above. To reasonably account for the core-hole effects [22], an Al $2p$ hole was introduced to a supercell consisting of approximately 100 atoms. The size of the supercell was sufficiently large to neglect the unrealistic interactions between the core holes [23]. The transition probabilities from the Al $2p$ to the unoccupied states were calculated within the electric dipole approximation. These were integrated over the whole Brillouin zone of the supercell using a $2 \times 2 \times 2$ k-point mesh. The transition energy of the theoretical spectrum was obtained from the difference of the total electronic energy of the supercell at the final core hole induced state and that of the ground state. The final spectrum was broadened by convoluting it with a Gaussian function with a full width at half maximum (FWHM) of 0.8 eV. The small energy splitting of 0.07 eV between the Al $2p_{1/2}$ and $2p_{3/2}$ levels was neglected for simplicity.

The chemical bonding differences probed by the spectral difference between AlH_3 and other Al containing compounds were analyzed based on Mulliken population analysis of atomic orbitals [24]. The PDOS, BOP, and effective charge were calculated by using the overlap integral between atomic orbitals and their coefficients for wavefunctions [25]. This population analysis of the OLCAO method aids intuitive understanding because it uses atomic orbital basis sets, which is one of the main benefits of the OLCAO method. PDOS was constructed by convoluting the orbital population with a Gaussian function (FWHM: 0.4 eV). We chose a smaller FWHM to clearly evaluate the atomic orbital contribution near the band gap.

4. Conclusions

We have investigated the chemical bonding of AlH_3 by means of Al- $L_{2,3}$ ELNES and its first-principles band calculation. The results obtained are summarized as follows:

- (1) Experimental Al- $L_{2,3}$ ELNES exhibited clear chemical shifts between metallic Al, AlH_3 , and Al_2O_3 . The threshold of the hydride spectrum was intermediate between those of Al and Al_2O_3 . The first-principles calculation reasonably reproduced the shape and chemical shift of the experimental spectra.
- (2) Theoretical chemical bonding data obtained by Mulliken population analysis of the calculated electronic structures revealed that the ionic bonding and covalent bonding strengths of the hydride were intermediate between those of Al and Al_2O_3 .

- (3) The theoretical Al- $L_{2,3}$ spectra and chemical bonding between the four Al compounds (Al, AlH₃, Al₂O₃, and AlF₃) exhibited systematic trends between the chemical bonding and their spectral features (fine peak structure and chemical shift). These trends are expected to be useful for further TEM-EELS nanoscale analysis of the chemical bonding changes that occur during the dehydrogenation of AlH₃ hydrides.

Acknowledgments

This work was supported in part by Grants-in-Aid for Scientific Research (KAKENHI) in Priority Areas (#474) “Atomic Scale Modification” from the Ministry of Education, Culture, Sports, Science and Technology (MEXT), Japan. We thank W.Y. Ching for allowing us to use the OLCAO code.

References

1. Sandrock, G.; Reilly, J.; Graetz, J.; Zhou, W.M.; Johnson, J.; Wegrzyn, J. Accelerated thermal decomposition of AlH₃ for hydrogen-fueled vehicles. *J. Appl. Phys. A* **2005**, *80*, 687–690.
2. Graetz, J.; Reilly, J.J. Decomposition Kinetics of the AlH₃ Polymorphs. *J. Phys. Chem. B* **2005**, *109*, 22181–22185.
3. Orimo, S.; Nakamori, Y.; Kato, T.; Brown, C.; Jensen, C.M. Intrinsic and mechanically modified thermal stabilities of α -, β - and α -aluminum trihydrides AlH₃. *Appl. Phys. A Mater.* **2006**, *83*, 5–8.
4. Ke, X.; Kuwabara, A.; Tanaka, I. Cubic and orthorhombic structures of aluminum hydride AlH₃ predicted by a first-principles study. *Phys. Rev. B* **2005**, *71*, 184107:1–184107:7.
5. Pickard, C.J.; Needs, R.J. Metallization of aluminum hydride at high pressures: A first-principles study. *Phys. Rev. B* **2007**, *76*, 144114:1–144114:5.
6. Graetz, J.; Chaudhuri, S.; Lee, Y.; Vogt, T.; Muckerman, J.T.; Reilly, J.J. Pressure-induced structural and electronic changes in α -AlH₃. *Phys. Rev. B* **2006**, *74*, 214114:1–214114:7.
7. Graetz, J.; Reilly, J.J. Thermodynamics of the α , β and γ polymorphs of AlH₃. *J. Alloys Comp.* **2006**, *424*, 262–265.
8. Brinks, H.W.; Langley, W.; Jensen, C.M.; Graetz, J.; Reilly, J.J.; Hauback, B.C. Synthesis and crystal structure of β -AlD₃. *J. Alloys Compounds* **2006**, *424*, 262–265.
9. Yartys, V.A.; Denys, R.V.; Maehlen, J.P.; Frommen, C.; Fichtner, M.; Bulychev, B.M.; Emerich, H. Double-bridge bonding of aluminium and hydrogen in the crystal structure of γ -AlH₃. *Inorg. Chem.* **2007**, *46*, 1051–1055
10. Vajeeston, P.; Ravindran, P.; Fjellvåg, H. Novel high pressure phases of β -alH₃: A density-functional study. *Chem. Mater.* **2008**, *20*, 5997–6002.
11. Takeda, Y.; Saitoh, Y.; Saitoh, H.; Machida, A.; Aoki, K.; Yamagami, H.; Muro, T.; Kato, Y.; Kinoshita, T. Electronic structure of aluminium trihydride studied using soft X-ray emission and absorption spectroscopy. *Phys. Rev. B* **2011**, *84*, 153102:1–153102:4.
12. Ikeda, K.; Muto, S.; Tatsumi, K.; Menjo, M.; Kato, S.; Bielman, M.; Züttel, A.; Jensen, C.M.; Orimo, S. Dehydrating reaction of AlH₃: *In situ* microscopic observations combined with thermal and surface analyses. *Nanotechnology* **2009**, *20*, 204004:1–204004:4.

13. Muto, S.; Tatsumi, K.; Ikeda, K.; Orimo, S. Dehydriding process of α -AlH₃ observed by transmission electron microscopy and electron energy-loss spectroscopy. *J. Appl. Phys.* **2009**, *105*, 123514:1–123514:4.
14. Keast, V.J.; Scott, A.J.; Kappers, M.J.; Foxon, C.T.; Humphreys, C.J. Electronic structure of GaN and In_xGa_{1-x}N measured with electron energy-loss spectroscopy *Phys. Rev. B* **2002**, *66*, 125319:1–125319:7.
15. Mauchamp, V.; Boucher, F.; Ouvrard, G.; Moreau, P. *Ab initio* simulation of the electron energy-loss near-edge structures at the Li K edge in Li, Li₂O, and LiMn₂O₄. *Phys. Rev. B* **2006**, *74*, 115106:1–115106:4.
16. Olovsson, W.; Tanaka, I.; Mizoguchi, T.; Radtke, G.; Puschnig, P.; Ambrosch-Draxl, C. Al L_{2,3} edge X-ray absorption spectra in III–V semiconductors: Many-body perturbation theory in comparison with experiment. *Phys. Rev. B* **2011**, *83*, 195206:1–195206:8.
17. Filippetti, K.; Spaldin, N.A. Self-interaction-corrected pseudopotential scheme for magnetic and strongly-correlated systems. *Phys. Rev. B* **2003**, *67*, 125109:1–125109:15.
18. Muto, S.; Puetter, R.C.; Tatsumi, K. Spectral restoration and energy resolution improvement of electron energy-loss spectra by Pixon reconstruction: I. Principle and test examples. *J. Electron Microsc.* **2006**, *55*, 215–223.
19. Kresse, G.; Furthmüller, J. Efficient iterative schemes for *ab initio* total-energy calculations using a plane-wave basis set. *Phys. Rev. B* **1996**, *54*, 11169–11181.
20. Kresse, G.; Joubert, D. From ultrasoft pseudopotentials to the projector augmented-wave method. *Phys. Rev. B* **1999**, *59*, 1758–1775.
21. Ching, W.Y. Theoretical studies of the electronic properties of ceramic materials. *J. Am. Ceram. Soc.* **1990**, *73*, 3135–3160.
22. Mo, S.D.; Ching, W.Y. *Ab initio* calculation of the core-hole effect in the electron energy-loss near-edge structure. *Phys. Rev. B* **2000**, *62*, 7901–7907.
23. Mogi, M.; Yamamoto, T.; Mizoguchi, T.; Tatasumi, K.; Yoshioka, S.; Kameyama, S.; Tanaka, I.; Adachi, H. Theoretical investigation of Al K-edge X-ray absorption spectra of Al, AlN and Al₂O₃ *Mater. Trans.* **2004**, *45*, 2031–2034.
24. Mulliken, R.S. Electronic population analysis on LCAO-MO molecular wave functions. *J. Chem. Phys.* **1955**, *23*, 1833–1840.
25. Mizoguchi, T.; Tatsumi, K.; Tanaka, I. Peak assignments of ELNES and XANES using overlap population diagrams. *Ultramicroscopy* **2006**, *106*, 1120–1128.